Steady squares and hexagons on a subcritical ramp

R. B. Hoyle*
Department of Applied Mathematics and Theoretical Physics, Univeristy of Cambridge, Cambridge CB3 9EW, United Kingdom
(Received 21 March 1994)

Steady squares and hexagons on a subcritical ramp are studied, both analytically and numerically, within the framework of the lowest-order amplitude equations. On the subcritical ramp, the external stress or control parameter varies continuously in space from subcritical to supercritical values. At the subcritical end of the ramp, pattern formation is suppressed, and patterns fade away into the conduction solution. It is shown that three-dimensional patterns may change shape on a subcritical ramp. A square pattern becomes a pattern of rolls as it fades, with the roll axes aligned in the direction orthogonal to that in which the control parameter varies. Hexagons in systems with horizontal midplane symmetry become a pattern of rectangles before reaching the conduction solution. There is a suggestion that hexagons in systems which lack this symmetry might fade away through a roll pattern. Numerical simulations are used to illustrate these phenomena.

PACS number(s): 47.20.Ky

I. INTRODUCTION

This paper concerns the behavior of square and hexagonal patterns subject to a space-varying external stress or control parameter. When the control parameter varies in space, connecting a subcritical to a supercritical region, the region of variation is known as a subcritical ramp. In the case of rolls, Kramer *et al.* [1] and Pomeau and Zaleski [2] have shown that when the control parameter varies slowly and smoothly in space, the subcritical ramp perfectly selects the pattern wavelength, i.e., the band of allowable wave numbers collapses to a single wave number. Riecke [3] has shown further that localized regions where the control parameter varies rapidly lead to deviations from this perfect selection. Malomed and Nepomnyashchy [4] considered rolls aligned at an arbitrary angle to the ramp and showed that rolls parallel to the slope of the subcritical ramp minimize the Lyapunov functional, whereas those orthogonal to the direction of variation, which correspond to the purely one-dimensional situation, maximize the functional. Malomed [5] showed that wave-number-selection effects also occur for one-dimensional traveling waves on a subcritical ramp, within the framework of both cubic and quintic complex Ginzburg-Landau equations.

The question of how subcritical ramps affect higher-dimensional patterns has not yet been explored. This paper is concerned not with wave-number selection, but with the changes in shape that stationary squares and hexagons at the critical wave number experience under the influence of a subcritical ramp. Both hexagons and squares are often observed in physical systems; see, for example, Hoyle [6], Golubitsky, Swift, and Knobloch [7], and references therein. In the context of Turing structures, Castets *et al.* [8] observed a pattern of hexagons fading into rolls in a region of varying reactant concentration during their experiments on nonequilibrium chemical patterns in a single-phase open reactor.

In this paper, the changing patterns are investigated using the appropriate lowest-order envelope equations, which were first introduced by Newell and Whitehead [9] and Segel [10], and the paper is organized as follows: Sec. II contains a theoretical analysis and Sec. III a numerical simulation of the behavior of a square pattern on a subcritical ramp, while Secs. IV and V contain the corresponding analyses for a supercritically bifurcating hexagonal pattern. The final Sec. VI contains a brief discussion of the results.

II. SQUARES ON A RAMP

Consider a square pattern revealed in the variations of a representative physical variable $f(x,y,t)$, for example, the fluid density in a convection experiment. The pattern varies in the horizontal x and y directions, and also in time t, and we shall assume that the physical variable can be written

$$f(x,y,t)=\tilde{A}(X,Y,T)e^{ik_c x}+\tilde{B}(X,Y,T)e^{ik_c y}+\text{c.c.}\ , \qquad (1)$$

where k_c is the critical wave number for the onset of instability, and the amplitudes $\tilde{A}$ and $\tilde{B}$ are functions of X, Y, and T, the long modulation scales in the x, y, and t directions, respectively. Close to the onset of the pattern-forming instability, the control parameter or external stress $\bar{r}$, for example, the Rayleigh number for a convecting fluid, is given by $\bar{r}=\epsilon^2 r$, say, where $\epsilon \ll 1$ and $r \sim O(1)$. If $X=\epsilon x$, $Y=\epsilon y$, $T=\epsilon^2 t$, $\tilde{A}=\epsilon A$, and $\tilde{B}=\epsilon B$, with $A \sim O(1)$ and $B \sim O(1)$, then the rescaled amplitudes A and B evolve according to the equations

$$A_T = rA - |A|^2 A - \lambda |B|^2 A + A_{XX} + \text{h.o.t.}\ , \qquad (2)$$

$$B_T = rB - |B|^2 B - \lambda |A|^2 B + B_{YY} + \text{h.o.t.}\ , \qquad (3)$$

*Present address: Department of Engineering Sciences and Applied Mathematics, Northwestern University, Evanston, IL 60208.

where the control parameter r is real and is assumed to be constant in space, λ is a real $O(1)$ constant, and h.o.t. stands here and hereafter for higher-order terms. These are essentially the same as the amplitude equations derived for three-dimensional patterns by Newell and Whitehead [9] and refined by Cross [11], except that here spatial derivatives of third and higher orders are neglected. The coefficients of the terms $|A|^2A$ and $|B|^2B$ must be negative if squares are to be a stable solution and can be set to -1 by rescaling the amplitudes. It can be shown that squares $A=R_0$, $B=R_0$, $R_0^2=r/(1+\lambda)$ are the stable, preferred pattern at the onset of instability for $r>0$ and $-1<\lambda<1$.

If the rescaled control parameter r is now allowed to vary slowly in space, so that $r\equiv r(X,Y)$, then to leading order r can be replaced by $r(X,Y)$ in the amplitude equations (Kramer *et al.* [1]; Pomeau and Zaleski [2]). The simplification, made below, that the control parameter r and the pattern amplitudes vary only in one direction restricts the analysis to the treatment of patterns at the critical wave number. However, the results should be valid at leading order since the analysis of rolls on a subcritical ramp (Kramer *et al.* [1]; Pomeau and Zaleski [2]) suggests that any wave-number-selection effect would occur at the next order in ϵ, i.e., the wave number k would be given by $k=k_c+\epsilon^2 q(X,Y,T)$ for some function $q(X,Y,T)$.

Choosing the X direction to be the one in which the control parameter varies, the physical variable can be represented by

$$f(x,y,t)=\tilde{A}(X,T)e^{ik_c x}+\tilde{B}(X,T)e^{ik_c y}+\text{c.c.}\ , \tag{4}$$

and the amplitudes A and B are governed by the equations

$$A_T=r(X)A-|A|^2A-\lambda|B|^2A+A_{XX}\ , \tag{5}$$

$$B_T=r(X)B-|B|^2B-\lambda|A|^2B\ . \tag{6}$$

These leading-order amplitude equations are derived from Eqs. (2) and (3), neglecting the higher-order terms and setting $\partial_Y=0$. We shall consider the situation where squares are stable at the bifurcation from the conduction solution $A=B=0$, so we must have $|\lambda|<1$.

Consider the situation where the control parameter $r(X)$ varies smoothly from subcritical $r(X)\to r_1<0$, as $X\to-\infty$, to supercritical $r(X)\to r_2>0$, as $X\to+\infty$. The boundary conditions on A and B are easy to determine. As $X\to-\infty$, the control parameter is subcritical, rolls and squares are unstable, and the conduction solutions is stable, so $A\to 0, B\to 0$. As $X\to+\infty$, the control parameter is supercritical, squares are stable, rolls and the conduction solution are unstable, so $|A|^2\to r_2/(1+\lambda), |B|^2\to r_2/(1+\lambda)$.

This system has a Lyapunov functional $V(T)$ given by

$$V=\langle r(X)|A|^2+r(X)|B|^2-\tfrac{1}{2}|A|^4 -\tfrac{1}{2}|B|^4-\lambda|B|^2|A|^2-|A_X|^2\rangle\ , \tag{7}$$

where $\langle\ \rangle$ represents a spatial average over a horizontal domain, which includes a "slice" of the ramp between $y=y_1$ and $y=y_2$ for any y_1 and y_2. The Lyapunov functional is always increasing with time since

$$V_T=2\langle|A_T|^2+|B_T|^2\rangle\geq 0\ . \tag{8}$$

It can be shown that $V\leq r_2^2/(1-|\lambda|)$. So V is increasing and bounded above, and therefore must tend to a stationary value $V\to V_0$. This corresponds to a steady solution for A and B.

Equation (6) can be rewritten

$$B_T=B\{r(X)-|B|^2-\lambda|A|^2\}\ . \tag{9}$$

The steady solutions for B then are $B=0$ and $|B|^2=r(X)-\lambda|A|^2$; the second solution only exists when $r(X)-\lambda|A|^2>0$. Linearizing around $B=0$ reveals that $B=0$ is a stable solution if $r(X)-\lambda|A|^2<0$ and unstable otherwise. Linearizing around $|B|^2=r(X)-\lambda|A|^2$ shows that this solution is stable to perturbations in B wherever it exists.

Consider the quantity $f(X)=r(X)-\lambda|A|^2$. As $X\to-\infty$, $f(X)\to r_1<0$, and as $X\to+\infty$, $f(X)\to r_2/(1+\lambda)>0$, but $f(X)$ must vary continuously, so at some $X=X_*$ we must have $f(X_*)=0$. Then, for $X<X_*$, the stable steady solution is $B=0$, and for $X>X_*$ it is $|B|^2=r(X)-\lambda|A|^2$; this solution is continuous at $X=X_*$. From Eq. (6) it is clear that $B(X,T)$ is not constrained to be smooth in X, so this solution is perfectly acceptable. It shall be assumed here that X_* is unique, so that B does not return to zero at any point when $X>X_*$, although it is possible that for some shapes of $r(X)$ this might happen.

If this solution for $|B|^2$ is substituted into the equation for A_T [Eq. (5)], and a steady solution $A_T=0$ is sought, then for $X<X_*$ Eq. (5) becomes

$$0=r(X)A-|A|^2A+A_{XX}\ , \tag{10}$$

with solution $A_1(X)$, say, and for $X>X_*$ it becomes

$$0=(1-\lambda)r(X)A-(1-\lambda^2)|A|^2A+A_{XX}\ , \tag{11}$$

with solution $A_2(X)$. The solution A_1 must satisfy the boundary condition as $X\to-\infty$, and A_2 must satisfy the boundary condition as $X\to+\infty$. Since the differential equations for A are second order in X, A and A_X must match at X_*. This must be possible since the existence of a Lyapunov functional guarantees the existence of a steady solution; it is achieved by varying X_* and any free parameters in A_1 and A_2.

At the very beginning, higher-order terms were neglected in the amplitude equations. In particular, derivatives of higher order than 2 were neglected. In formulating the amplitude equations, it was assumed that the pattern would only be modulated on long space and time scales. However, close to $X=X_*$, the modulation is rapid in space, and the higher-order derivatives will lead to corrections to the "outer" solution found above. All but one of the higher-order derivative terms will not become important until $\partial_X\simeq O(\epsilon^{-1})$, i.e., until the assumptions that led to the amplitude equations in the first place break down. However, there are currently no spatial derivatives at all in Eq. (6); the first correction to this

equation is to add a term $-\epsilon^2 B_{XXXX}/4$ to the right hand side. This correction becomes important before $\partial_X \simeq O(\epsilon^{-1})$. The corrected version of Eq. (6) for steady solutions is

$$O = r(X)B - |B|^2 B - \lambda |A|^2 B - \frac{\epsilon^2}{4} B_{XXXX} \ . \tag{12}$$

In the inner region close to $X = X_*$, the control parameter $r(X)$ and the square of the amplitude $|A|^2(X)$ can be expanded in Taylor series about $X = X_*$. Writing $r(X_*) = r_*$, this gives

$$r(X) = r_* + (X - X_*) \frac{\partial r}{\partial X}\bigg|_{X=X_*} + \cdots \tag{13}$$

$$|A|^2(X) = \frac{r_*}{\lambda} + (X - X_*) \frac{\partial |A|^2}{\partial X}\bigg|_{X=X_*} + \cdots \ . \tag{14}$$

Substituting these expressions into Eq. (12) gives

$$0 = \{c(X - X_*) - |B|^2\} B - \frac{\epsilon^2}{4} B_{XXXX} + \cdots \ , \tag{15}$$

where

$$c = \frac{\partial r}{\partial X}\bigg|_{X=X_*} - \lambda \frac{\partial |A|^2}{\partial X}\bigg|_{X=X_*} \ . \tag{16}$$

If $(X - X_*)$ is now rescaled by ϵ^a, and B by ϵ^b, then for all the terms in Eq. (15) to be of the same order, it is required that $a = \frac{2}{5}$ and $b = \frac{1}{5}$. So as stated above, the correction comes in before $\partial_X \simeq O(\epsilon^{-1})$. The correction to the amplitude is $O(\epsilon^{1/5})$, which is smaller than the $O(1)$ outer solution as $\epsilon \to 0$, and so there are no singularities generated in the inner solution. Therefore, the outer solution found above is a good approximation. This scaling is very similar to that found by Manneville and Pomeau [12] for a grain boundary between two orthogonal sets of rolls in an isotropic environment.

The outer solution, has the interesting feature that when $|A|^2 = r_*/\lambda$, $B = 0$. So $|A|$ will be positive when B is zero, over at least a small range of X, except in the special case when r_* turns out to be zero. Over this small range of X an observer will see rolls with their axes aligned along the y axis instead of squares. A square pattern on a subcritical ramp will become a pattern of rolls before it fades away into the conduction solution. The roll axes will be aligned in the direction orthogonal to that in which the control parameter varies.

III. NUMERICAL RESULTS FOR SQUARES ON A RAMP

A numerical integration of the following equations,

$$A_T = r(\rho)A - |A|^2 A - \lambda |B|^2 A + A_{XX} \ , \tag{17}$$

$$B_T = r(\rho)B - |B|^2 B - \lambda |A|^2 B + B_{YY} \ , \tag{18}$$

is performed, using a pseudospectral code on a square grid with 100 modes in each direction. The control parameter takes the form $r(\rho) = 1 + 3 \tanh 10(x_0 - \rho)$, where $\rho = \sqrt{X^2 + Y^2}$, and $x_0 = 10\pi$. Note that $r(\rho) < 0$ for $\rho > x_0 + (\frac{1}{10})\tanh^{-1}(\frac{1}{3}) \simeq 10.01\pi$, and $r(\rho) > 0$ for $\rho < x_0 + (\frac{1}{10})\tanh^{-1}(\frac{1}{3})$. The system is in the parameter regime where squares are stable since $\lambda = 0.5$. The domain of integration is $-2x_0 < X < 2x_0$ and $-2x_0 < Y < 2x_0$. The control parameter is chosen to vary radially so that the boundary conditions are approximately periodic in the X and Y directions.

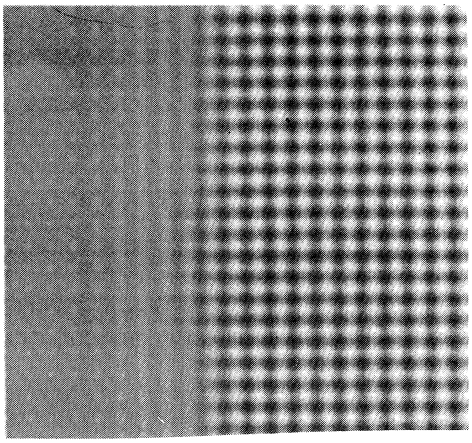

FIG. 1. Grey scale plot of $f(x,y,t) = \tilde{A}(X,Y)e^{ik_c x} + \tilde{B}(X,Y)e^{ik_c y} + \text{c.c.}$ in the region $-1.2x_0 < X < -0.8x_0$, $-0.2x_0 < Y < 0.2x_0$, with a subcritical ramp at $X \simeq -x_0$, where $x_0 = 10\pi$.

The initial profiles for the amplitudes are $A(X,Y) = B(X,Y) = \sqrt{\frac{8}{3}}$, which is the approximate steady solution as $\rho \to 0$. The amplitude equations (17) and (18) are then integrated forward in time to find the true steady solution. Figure 1 shows the reconstructed pattern $f(x,y,t) = \tilde{A}(X,Y)e^{ik_c x} + \tilde{B}(X,Y)e^{ik_c y} + \text{c.c.}$ in the small region $-1.2x_0 < X < -0.8x_0$, $-0.2x_0 < Y < 0.2x_0$, on the ramp where A and B are the steady solutions found by integration. The critical wave number is $k_c = 10$. The region shown in Fig. 1 is small enough that the circular boundary $\rho = x_0 + (\frac{1}{10})\tanh^{-1}(\frac{1}{3})$, at which the control parameter r is zero, looks approximately like the straight line $X = -x_0 - (\frac{1}{10})\tanh^{-1}(\frac{1}{3})$, so the theory developed in the preceding section should apply here.

The numerical reconstruction shows a fully developed square pattern in the supercritical region ($r > 0$) to the right of $X = -x_0 - (\frac{1}{10})\tanh^{-1}(\frac{1}{3})$, which changes into a pattern of rolls parallel to the Y axis close to $X = -x_0 - (\frac{1}{10})\tanh^{-1}(\frac{1}{3})$ (where $r = 0$) and then fades away into the conduction solution in the subcritical region ($r < 0$) to the left of $X = -x_0 - (\frac{1}{10})\tanh^{-1}(\frac{1}{3})$. This is exactly what theory predicts.

A closer examination of the X and Y roll amplitudes shows that both A and B are real [numerically $\text{Im}(A)$ and $\text{Im}(B)$ are $O(10^{-16})$], so there is no phase winding at lowest order, and that B does indeed decay to zero faster than A as $X \to -2x_0$ (Fig. 2). There is also some adjustment of the amplitudes at the supercritical edge of the ramp $X = -x_0 - (\frac{1}{10})\tanh^{-1}(\frac{1}{3}) + \delta$, where $0 < \delta \ll 1$, but

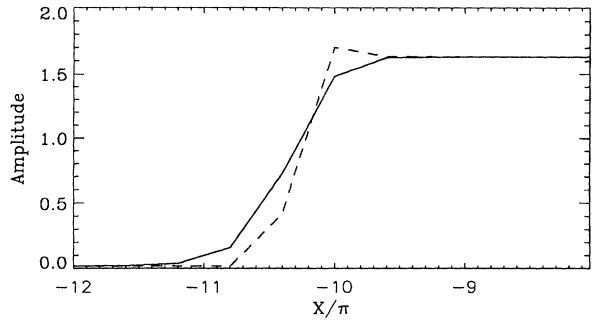

FIG. 2. Plots of the X- and Y-roll amplitudes, A and B, respectively, across a subcritical ramp. The solid curve shows $A(X,Y=0)$ and the dotted curve shows $B(X,Y=0)$. At $Y=0$, the control parameter r is zero at $X=-10\pi$, positive for $X\gtrsim-10\pi$, and negative for $X\lesssim-10\pi$. The curves appear jagged because there are only a few integration points in the region shown on the plot.

this has less effect on the overall pattern, since A and B are of comparable size there.

IV. HEXAGONS ON A RAMP

Consider a steady hexagonal pattern. The physical variable f, in whose variations the pattern is revealed, can be represented as

$$f(x,y,t)=\tilde{A}(X,Y,T)e^{ik_c x}+\tilde{B}(X,Y,T)e^{ik_c(-x+\sqrt{3}y)/2}+\tilde{C}(X,Y,T)e^{ik_c(-x-\sqrt{3}y)/2}+\text{c.c.}\ , \tag{19}$$

where k_c is the critical wave number for the onset of the pattern-forming instability, and X, Y, and T are long modulation scales in the x, y, and t directions as before. Again, close to onset the control parameter $\tilde{r}$ is given by $\tilde{r}=\epsilon^2 r$ and if $X=\epsilon x$, $Y=\epsilon y$, $T=\epsilon^2 t$, $\tilde{A}=\epsilon A$, $\tilde{B}=\epsilon B$, and $\tilde{C}=\epsilon C$, then the rescaled amplitudes A, B, and C evolve according to the equations

$$A_T=rA+\alpha\bar{B}\bar{C}-\nu_1|A|^2A-\nu_2(|B|^2+|C|^2)A+A_{XX}\ , \tag{20}$$

$$B_T=rB+\alpha\bar{A}\bar{C}-\nu_1|B|^2B-\nu_2(|C|^2+|A|^2)B+\tfrac{1}{4}(\partial_X-\sqrt{3}\partial_Y)^2B\ , \tag{21}$$

$$C_T=rC+\alpha\bar{A}\bar{B}-\nu_1|C|^2C-\nu_2(|A|^2+|B|^2)C+\tfrac{1}{4}(\partial_X+\sqrt{3}\partial_Y)^2C\ , \tag{22}$$

where the control parameter r is real $O(1)$ and constant in space, α is a real constant of size $O(\epsilon)$ before rescaling, ν_1 and ν_2 are real $O(1)$ constants, and higher-order terms have been neglected. Again, these are of the same form as the envelope equations derived for three-dimensional patterns by Newell and Whitehead [9], except that spatial derivatives of higher order than 2 are neglected.

If the control parameter varies in space, then to leading order, r can be replaced by $r(X,Y)$ in the amplitude equations. This time the ramp is chosen to vary in the Y direction, and the amplitudes A, B, and C are assumed to vary in the Y direction only. The physical variable is now given by

$$f(x,y,t)=\tilde{A}(Y,T)e^{ik_c x}+\tilde{B}(Y,T)e^{ik_c(-x+\sqrt{3}y)/2}+\tilde{C}(Y,T)e^{ik_c(-x-\sqrt{3}y)/2}+\text{c.c.} \tag{23}$$

and the relevant amplitude equations are

$$A_T=r(Y)A+\alpha\bar{B}\bar{C}-\nu_1|A|^2A-\nu_2(|B|^2+|C|^2)A\ , \tag{24}$$

$$B_T=r(Y)B+\alpha\bar{A}\bar{C}-\nu_1|B|^2B-\nu_2(|C|^2+|A|^2)B+\tfrac{3}{4}\partial_Y^2B\ , \tag{25}$$

$$C_T=r(Y)C+\alpha\bar{A}\bar{B}-\nu_1|C|^2C-\nu_2(|A|^2+|B|^2)C+\tfrac{3}{4}\partial_Y^2C\ . \tag{26}$$

These equations are derived from Eqs. (20), (21), and (22), setting $\partial_X=0$. The control parameter $r(Y)$ is assumed to be real, varying from subcritical $[r(Y)\to r_1<0]$ at $Y\to-\infty$ to supercritical $[r(Y)\to r_2>0]$ at $Y\to+\infty$. If $\alpha\neq0$, the system is not invariant under the transformation $f\to-f$, whereas if $\alpha=0$, it is. This invariance is equivalent to symmetry under reflection in the midplane in a convecting layer (see, for example, Golubitsky, Swift and Knobloch [7]).

Let us consider the asymmetric case $\alpha\neq0$. Without loss of generality, α can be chosen to be positive, since the problem can always be reduced to this case by means of the transformation $f\to-f$. If $(\nu_1+2\nu_2)>0$, then hexagons bifurcate transcritically from the trivial solution, and there is a branch of stable hexagons $[A=B=C=R_0,\ r_2+\alpha R_0-(\nu_1+2\nu_2)R_0^2=0]$ in the region $r>-\alpha^2/4(\nu_1+2\nu_2)$ and $r<\infty$ (if $\nu_1>\nu_2$) or $r<\alpha^2(2\nu_1+\nu_2)/(\nu_1-\nu_2)^2$ (if $\nu_1<\nu_2$). If $r_1<-\alpha^2/4(\nu_1+2\nu_2)$, then as $Y\to-\infty$, the conduction solution will be stable, and if $\nu_1>\nu_2$, or if $\nu_1<\nu_2$ and $r_2<\alpha^2(2\nu_1+\nu_2)/(\nu_1-\nu_2)^2$, then as $Y\to+\infty$, steady hexagons will be stable. This situation is much harder to analyze than the square case. If it is assumed that $B(Y)=C(Y)$ for the steady solution, which symmetry would suggest, then it is clear from Eq. (24) that $A=0$ implies $B=C=0$ if $\alpha\neq0$, and so the analogous situation to that described above for squares cannot occur. However, $B=C=0$ does not imply $A=0$, so a region of rolls is possible, and this suggests, although in no way demonstrates, that the hexagonal pattern might fade away into the conduction solution via a pattern of rolls. In this case, however, the rolls would lie parallel to the Y axis, and not, as experimental observation [8] would suggest, perpendicular to it.

If there is symmetry under reflection in a horizontal midplane, for example, convection in a Boussinesq fluid with identical boundary conditions on the top and bottom plates, we have $\alpha=0$. If $\nu_1+2\nu_2>0$, then hexagons bifurcate supercritically from the trivial solution. If, also, $\nu_1>\nu_2$ (note that this implies $\nu_1>0$), then steady hexagons at the critical wave number are stable for $r>0$, and the analysis is very similar to the analysis in the square case.

There is a Lyapunov functional $V(T)$ given by

$$V(T)=\langle r(Y)(|A|^2+|B|^2+|C|^2)-\frac{\nu_1}{2}(|A|^4+|B|^4+|C|^4)\rangle$$
$$+\langle -\nu_2(|A|^2|B|^2+|B|^2|C|^2+|C|^2|A|^2)-\tfrac{3}{4}(|B_Y|^2+|C_Y|^2)\rangle \ . \quad (27)$$

This is always increasing since

$$V_T=2\langle |A_T|^2+|B_T|^2+|C_T|^2\rangle \geq 0 \ . \quad (28)$$

It can also be shown that V is bounded above by $3r_2^2/2(\nu_1-\nu_2)$ for $\nu_2>0$, and by $3r_2^2/2(\nu_1+2\nu_2)$ for $\nu_2<0$. So V is increasing and bounded above and therefore must tend to a stationary value $V\to V_0$. This corresponds to a steady solution for A, B, and C.

Under the assumption that $B(Y)=C(Y)$ for the steady solution, it is found that for $Y<Y_*$, the amplitudes A and B satisfy the equations

$$A=0 \ , \quad (29)$$

$$r(Y)B-(\nu_1+\nu_2)|B|^2B+\tfrac{3}{4}B_{YY}=0 \ , \quad (30)$$

and for $Y>Y_*$,

$$|A|^2=\frac{1}{\nu_1}\{r(Y)-2\nu_2|B|^2\} \ , \quad (31)$$

$$0=\frac{(\nu_1-\nu_2)}{\nu_1}r(Y)B-\frac{(\nu_1-\nu_2)(\nu_1+2\nu_2)}{\nu_1}|B|^2B+\tfrac{3}{4}B_{YY} \ . \quad (32)$$

The rest of the analysis goes through in the same manner as for the square case, and it is found that at $Y=Y_*$, $A=0$, but $|B|^2=|C|^2=r_*/2\nu_2\geq 0$.

This shows $|B|$ and $|C|$ will be positive when A is zero, over a small range of Y close to Y_*, except in the special case when r_* turns out to be zero. In this region, an observer would expect to see rectangles instead of hexagons.

V. NUMERICAL RESULTS FOR HEXAGONS ON A RAMP

A numerical integration of the following equations,

$$A_T=r(\rho)A-\nu_1|A|^2A-\nu_2(|B|^2+|C|^2)A+A_{XX} \ , \quad (33)$$

$$B_T=r(\rho)B-\nu_1|B|^2B-\nu_2(|C|^2+|A|^2)B$$
$$+\tfrac{1}{4}(\partial_X-\sqrt{3}\partial_Y)^2B \ , \quad (34)$$

$$C_T=r(\rho)C-\nu_1|C|^2C-\nu_2(|A|^2+|B|^2)C$$
$$+\tfrac{1}{4}(\partial_X+\sqrt{3}\partial_Y)^2C \ , \quad (35)$$

is performed using a pseudospectral code on a square grid with 100 modes in each direction. The control parameter takes the form $r(\rho)=1+3\tanh 10(y_0-\rho)$, where $\rho=\sqrt{X^2+Y^2}$, and $y_0=10\pi$. This is very similar to that used in the square case, and it can be seen that $r(\rho)<0$ for $\rho>y_0+(\frac{1}{10})\tanh^{-1}(\frac{1}{3})\simeq 10.01\pi$, and $r(\rho)>0$ for $\rho<y_0+(\frac{1}{10})\tanh^{-1}(\frac{1}{3})$. Here $\nu_1=2$ and $\nu_2=1$, so that steady hexagons at the critical wave number are stable. The domain of integration is $-2y_0<X<2y_0$ and $-4y_0/\sqrt{3}<Y<4y_0/\sqrt{3}$. The control parameter is chosen to vary radially once more, so that the boundary conditions are approximately periodic in the X and Y directions.

The initial profiles for the amplitudes are $A(X,Y)=B(X,Y)=C(X,Y)=1$, which is the approximate steady solution as $\rho\to 0$. The amplitude equations (33), (34), and (35) are then integrated forward in time to find the true steady solution, in the same way as for squares. The moduli of the steady solutions, A, B, and C, at $X=0$ and for $-12.0\pi<Y<-7.5\pi$, are shown in Fig. 3. The middle point of the subcritical ramp, where $r=0$, is at $Y\simeq -10\pi$. In this region, the subcritical ramp is approximately straight and aligned along the X axis, so the theory developed in the preceding section should apply. It can be seen that the curve for $|B|$ lies on top of that for $|C|$ and also that $|A|$ does decay to zero faster than $|B|$ and $|C|$ as $Y\to -4y_0/\sqrt{3}$, as suggested by the theory. The amplitudes A, B, and C are approximately real [numerically, $\mathrm{Im}(A)$ is $O(10^{-16})$ and $\mathrm{Im}(B)$ and $\mathrm{Im}(C)$ are $O(10^{-2})$], so there is no phase winding at lowest order. The larger order of magnitude for $\mathrm{Im}(B)$ and $\mathrm{Im}(C)$, as compared to $\mathrm{Im}(A)$, probably arises from the curvature of the subcritical ramp. These results suggest that a hexagonal pattern changes into a pattern of rectangles as it fades away into the conduction solution, just as theory predicts.

Figure 4 shows the reconstructed pattern

$$f(x,y,t)=\tilde{A}(X,Y)e^{ik_c x}+\tilde{B}(X,Y)e^{ik_c(-x+\sqrt{3}y)/2}$$
$$+\tilde{C}(X,Y)e^{-ik_c(x+\sqrt{3}y)/2}+\text{c.c.}$$

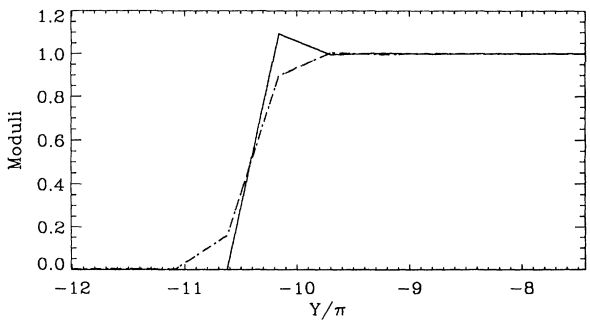

FIG. 3. Plots of the three roll amplitudes, A, B, and C, for a hexagonal pattern on a subcritical ramp. The solid, dotted, and dashed lines show the moduli of $A(X=0,Y)$, $B(X=0,Y)$, and $C(X=0,Y)$, respectively. At $X=0$, the control parameter is negative for $Y\lesssim -10\pi$ and positive for $Y\gtrsim -10\pi$. The curves appear jagged as in Fig. 2 because the region of the plot only includes a small number of integration points.

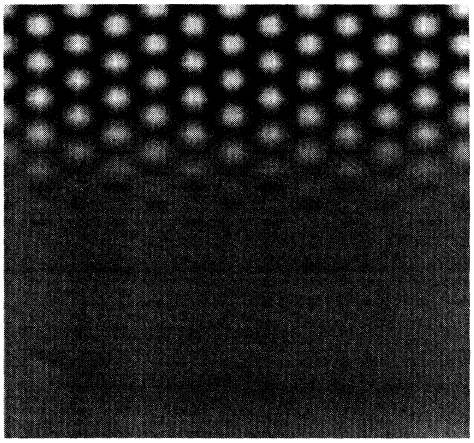

FIG. 4. Grey scale plot of $f(x,y,t)=\tilde{A}(X,Y)e^{ik_c x}+\tilde{B}(X,Y)e^{ik_c(-x+\sqrt{3}y)/2}+\tilde{C}(X,Y)e^{-ik_c(x+\sqrt{3}y)/2}+\text{c.c.}$ in the region $-0.1y_0<X<0.1y_0$, $-1.2y_0<Y<-0.97y_0$, with a subcritical ramp at $Y\simeq -y_0$ where $y_0=10\pi$.

in the small region $-0.1y_0<X<0.1y_0$, $-1.2y_0<Y<-0.97y_0$, on the ramp, where A, B, and C are the steady solutions found by integration. The critical wave number is $k_c=12$. The region shown in Fig. 4 is small enough that the circular boundary $\rho=y_0+(\frac{1}{10})\tanh^{-1}(\frac{1}{3})$, where $r=0$, appears to be a straight line $Y=-y_0-(\frac{1}{10})\tanh^{-1}(\frac{1}{3})$. The hexagonal pattern changes into a pattern of rectangles (barely visible on the plot) as it fades away into the conduction solution, just as predicted by the theory.

VI. DISCUSSION

The results in this paper show that three-dimensional patterns on a subcritical ramp may change shape as they fade away into the conduction solution. A square pattern becomes a pattern of rolls before it reaches the conduction solution. The roll axes are aligned in the direction orthogonal to that in which the control parameter varies.

For hexagons, the situation is more complicated. In systems without symmetry under reflection in the horizontal midplane, the lowest-order amplitude equations suggest that hexagons might change into a pattern of rolls on the ramp. In systems with the midplane symmetry, hexagons become a pattern of rectangles before fading away into the conduction solution.

ACKNOWLEDGMENTS

I thank Dr. M.R.E. Proctor for helpful discussions. I gratefully acknowledge the financial support of the Science and Engineering Research Council.

[1] L. Kramer, E. Ben-Jacob, H. Brand, and M. C. Cross, Phys. Rev. Lett. **49**, 1891 (1982).
[2] Y. Pomeau and S. Zaleski, J. Phys. (Paris) Lett. **44**, L135 (1983).
[3] H. Riecke, Europhys. Lett. **2**, 1 (1986).
[4] B. A. Malomed and A. A. Nepomnyashchy, Europhys. Lett. **21**, 195 (1993).
[5] B. A. Malomed, Phys. Rev. E **47**, 2257 (1993).
[6] R. B. Hoyle, Physica D **67**, 198 (1993).
[7] M. Golubitsky, J. W. Swift, and E. Knobloch, Physica D **10**, 249 (1984).
[8] V. Castets, E. Dulos, J. Boissonade, and P. De Kepper, Phys. Rev. Lett. **64**, 2953 (1990).
[9] A. C. Newell and J. A. Whitehead, J. Fluid Mech. **38**, 279 (1969).
[10] L. A. Segel, J. Fluid Mech. **38**, 203 (1969).
[11] M. C. Cross, Phys. Fluids **23**, 1727 (1980).
[12] P. Manneville and Y. Pomeau, Philos. Mag. A **48**, 607 (1983).

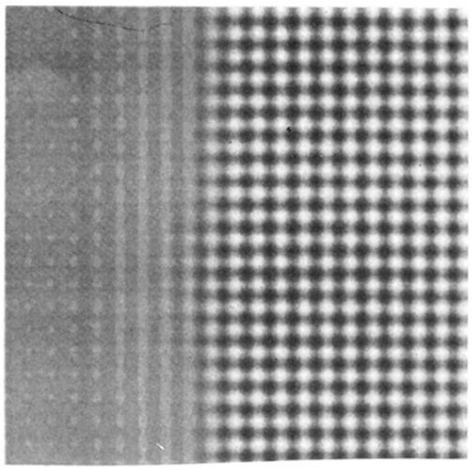

FIG. 1. Grey scale plot of $f(x,y,t)=\tilde{A}(X,Y)e^{ik_c x}+\tilde{B}(X,Y)e^{ik_c y}+\text{c.c.}$ in the region $-1.2x_0<X<-0.8x_0$, $-0.2x_0<Y<0.2x_0$, with a subcritical ramp at $X\simeq -x_0$, where $x_0=10\pi$.

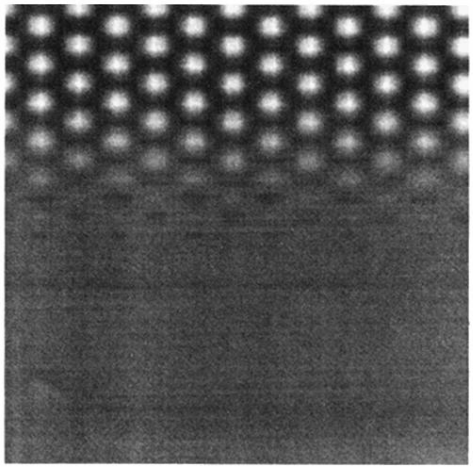

FIG. 4. Grey scale plot of $f(x,y,t)=\tilde{A}(X,Y)e^{ik_c x}+\tilde{B}(X,Y)e^{ik_c(-x+\sqrt{3}y)/2}+\tilde{C}(X,Y)e^{-ik_c(x+\sqrt{3}y)/2}+$c.c. in the region $-0.1y_0<X<0.1y_0$, $-1.2y_0<Y<-0.97y_0$, with a subcritical ramp at $Y\simeq -y_0$ where $y_0=10\pi$.